2022

Investigation of the electrocatalytic mechanisms of urea oxidation reaction on the surface of transition metal oxides

Xiaoying Lu

Journal of Colloid and Interface Science 620 (2022) 442–453

Contents lists available at ScienceDirect

Journal of Colloid and Interface Science

journal homepage: www.elsevier.com/locate/jcis

Investigation of the electrocatalytic mechanisms of urea oxidation reaction on the surface of transition metal oxides

Jianhua Ge [a], Zhongfei Liu [a], Minghui Guan [a], Juner Kuang [a], Yuhua Xiao [a], Yang Yang [a], Chi Him Tsang [b], Xiaoying Lu [b,*], Chunzhen Yang [a,*]

[a] School of Materials, Sun Yat-Sen University, Guangzhou 510275, PR China
[b] Faculty of Science and Technology, Technological and Higher Education Institute of Hong Kong, Hong Kong, PR China

GRAPHICAL ABSTRACT

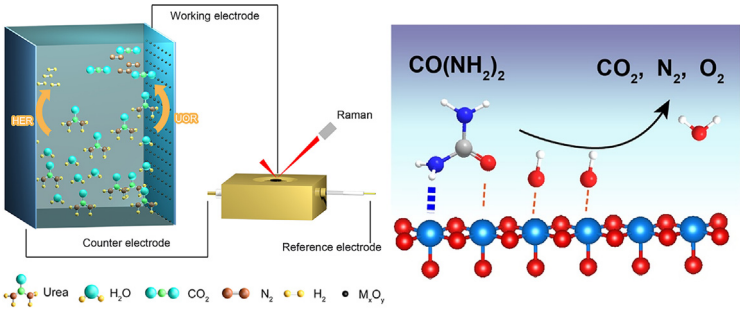

ARTICLE INFO

Article history:
Received 13 February 2022
Revised 23 March 2022
Accepted 31 March 2022
Available online 2 April 2022

Keywords:
urea oxidation reaction (UOR)
Solid–liquid Interfaces
Operando Raman spectroscopy
Surface adsorption energy

ABSTRACT

Urea oxidation reaction (UOR) has been widely considered as an alternative anodic reaction to water oxidation for the green production of hydrogen fuel. Due to the high catalytic activity of transition metal oxides towards UOR, various strategies have been developed to improve their syntheses and catalytic properties. However, little is known about the underlying mechanisms of UOR on catalyst surface. In this work, three transition metal oxides, including NiO, Co_3O_4, and Fe_2O_3 are investigated as model catalysts. Through analyzing the electrochemical properties by cyclic voltammetry (CV), electrochemical impedance spectroscopy (EIS), and *operando* Raman spectroscopy, it is revealed that NiO has a unique high catalytic activity towards UOR due to simultaneous formation of a thin layer of oxyhydroxide species above 1.40 V vs. RHE in alkaline media. In addition, density functional theory (DFT) calculations further suggest that the adsorption of urea molecules is largely affected by surface interactions resulting in different space configurations, which impose large influences on the consecutive deprotonation and N—N formation processes. Overall, results of this work point to the subtle adsorption – kinetics relationship in UOR and highlight the importance of the interfacial electronic interactions on catalyst surface.

1. Introduction

Electrocatalytic water splitting is one of the most promising approaches for hydrogen fuel production, which has been considered as a key technique to realize the sustainable development of clean and renewable energies for human society [1]. At the core of this technology lies the development of efficient catalysts to improve the kinetics of the oxygen evolution reaction (OER), which oxidizes water generating oxygen molecules on the anode of the electrolytic cell. However, even utilizing the state-of-the-art catalysts such as IrO_2 and RuO_2, the overall water electrolysis still

* Corresponding authors.
E-mail addresses: xylu@thei.edu.hk (X. Lu), yangchzh6@mail.sysu.edu.cn (C. Yang).

https://doi.org/10.1016/j.jcis.2022.03.152
0021-9797/

requires high energy consumption and operation cost to overcome the sluggish kinetics of OER [2]. An alternative approach is to replace OER with more thermodynamical favorable reactions at the anode, such as oxidation of ammonia [3], hydrazine [4], alcohol [5], glucose [6], and urea [7] to assist water electrolysis with low overpotentials and energy input. Among these reactions, the urea oxidation reaction (UOR) has attracted substantial research interests owning to its advantage in simultaneously remediating urine-rich waste water and hydrogen production. Comparing to the hydrogen evolution reaction (HER) at the cathode, the UOR still faces relatively large overpotentials. There are 6 consecutive proton-coupled electron transfer step (PCET) [8] involved in the presence of OH^- groups for complete oxidation of urea in order to generate N_2 and CO_2 according to the following electrode half-reactions: $CO(NH_2)_{2(aq)} + 6OH^-_{(aq)} \rightarrow N_{2(g)} + 5H_2O_{(aq)} + CO_{2(g)} + 6e^-$. Clearly, the development of highly efficient catalysts for UOR is of significance, thus considerable research efforts have been put forth to the exploration of different electrode materials to improve the kinetics of urea electro-oxidation [9].

So far, various transition metal-based catalysts such as IrO_2 [10], Pt-Ir [11], Ta_2O_5-IrO_2 [12], $Ni(OH)_2$ [13,14], Ni-Rh [11], $NiCo_2O_4$ [15], $NiMoO_4$ [16] and etc. have been implemented for urea oxidation which have demonstrated modest activities in either neutral or alkaline medium. Due to the high cost and limiting supply, noble metal catalysts such as Pt, Ru, or Ir-based catalysts are generally considered not suitable for large-scale industrial applications. Instead, Ni-/Co–/Fe-based catalysts have garnered tremendous research attention considering their earth abundance, high stability in the strong alkaline media, low cost, and etc. [17–19]. Indeed, they have demonstrated excellent electrocatalytic activities in various electrochemical reactions, including the oxygen reduction reaction (ORR) [20], the oxygen evolution reaction (OER) [21], CO_2 reduction reaction (CO_2RR) [22], and etc. Not only due to their innate electrochemical activities, but also the enriched structural diversity, as well as the ability to be mixed, doped, and combined with other materials, Ni-/Co–/Fe-based catalysts have been extensively investigated and often employed as model catalysts for the study of fundamental electrochemical processes and mechanisms. In this regard, we attempted to investigate the UOR mechanisms by using some representative examples of Ni, Fe and Co oxides and (oxy)hydroxides. Results may help us to establish a more intimate connection between the dissociation of urea molecules and heterogeneous catalyst systems.

So far, two major strategies have been explored to boost the UOR kinetics. One is to enhance the electrochemically active surface area (ECSA) by engineering the nanotechnology to increase the reactive metal sites exposed to electrolyte [23–25], and the other is to incorporate additional elements such as Pt, Cu, Mo and etc. [26–28] The doped elements can greatly promote the doping effect and modulate the electronic structure [29–32]. However, there is still lack of deep understanding of the underlying UOR mechanism. One significant question hasn't been answered is why Ni demonstrated such a unique promising intrinsic catalytic activity towards UOR. So far, there are few studies on the active sites and evolution of transition metal oxide surfaces in UOR reactions [33]. Understanding the specific interactions between urea and Ni catalytic sites would provide insights into the solid–liquid interfaces. The accurate determination of adsorption energy between catalytic intermediates and reactants will greatly benefit to the setup of property-activity correlations and the design of highly efficient UOR catalysts.

In this work, three commercially available transition metal oxides including rock-salt structured NiO, spinel-type Co_3O_4 and hematite α-Fe_2O_3, are employed as model catalysts for UOR. Their electrocatalytic behaviors at different electrochemical potentials for both OER and UOR are studied by cyclic voltammetry (CV) and electrochemical impedance spectroscopy (EIS). *Operando* Raman spectroscopy was conducted to probe the structure evolution and surface intermediates involved in UOR. To understand the surface interactions between catalysts and electrolyte, the adsorption energies of urea on different transition metal oxides were calculated by density functional theory (DFT) method. The adsorption energy of urea molecule on different catalyst surface can be largely affected by the electronic interactions, which results in different space configurations and influence the following decomposition process. Overall, results of this work revealed the complexity of the UOR mechanism.

2. Experimental

2.1. Materials

Nickel oxide (NiO) and Ferric oxide (Fe_2O_3) powders were purchased from Aladdin Reagent. Cobalt oxide (Co_3O_4) powder was bought from Alfa Aesar Chemical Co., LTD. $Ni(NO_3)_2{\cdot}6H_2O$, $Co(NO_3)_2{\cdot}6H_2O$ and $FeCl_3{\cdot}6H_2O$ from Aladdin Reagent were used for electrodeposition of hydroxide films. Potassium hydroxide (KOH) and Urea were brought from Sinopharm Chemical Reagent Co., Ltd. Nafion was ordered from Alfa Aesar Chemical Co., LTD. Ag/AgCl reference electrode was brought from CHI760e, Shanghai. Carbon paper was brought from Toray. All materials were used as received without further purification. Ultrapure water (18 M ohm) was used throughout this study.

2.2. Characterization

The powder X-ray diffraction (XRD) patterns of the samples were collected on a Bruker D8 Advance Powder X-ray diffractometer (45 kV, 30 mA) using Ni-filtered Cu Kα radiation in the 2θ ranging from 20 to 80° at a scan rate of 0.02° per second. The morphology of catalyst was observed by transmission electron microscope (TEM). The specific surface area of each oxide was determined using Brunauer, Emmet and Teller (BET) analysis carried out on a Micromeritics ASAP2020 equipment (Micromeritics Instrument Corp., USA). Samples were firstly degassed in vacuum at 473 K for 2 h, then the nitrogen adsorption and desorption isotherms were measured at 77 K and 273 K, respectively. The X-ray photoelectron spectroscopy (XPS) was carried out on ESCALab MKII X-ray photoelectron spectrometer. *Operando* Raman spectra were collected at room temperature (25℃) in a home-made electrochemical cell with a confocal Raman microscope (Renishaw inVia) using a laser with a wavelength of 532 as the excitation source. The laser power was 5 mW. The Raman electrolysis cell is designed with three electrodes. The electrode potential was stepwise increased from 1.2 V to 1.65 V with a voltage interval of 50 mV. *In situ* electrochemical gas chromatography is conducted with Shimadzu GC-2030 and thermal conductivity detector (TCD). Ar was used as the carrier gas for sampling the gas produced by electrochemical reaction. Before the reaction, Ar was purged into the electrochemical reaction cell and the electrolyte for 15 min. The electrode was applied at certain potentials for 10 min.

2.3. Electrochemical measurements

The electrochemical experiments were performed in a standard three-electrode configuration by using an electrochemical workstation (CHI760e, Shanghai). A Pt plate, and saturated Ag/AgCl

electrode were used as counter electrode (CE) and reference electrode (RE), respectively. Both glass carbon electrode and carbon paper were employed as working electrode (WE) depending on the experiment purpose.

For transition metal oxides, electrodes were prepared by the classical drop-casting method. For catalyst ink preparation, 5 mg of catalysts (NiO, Fe_2O_3, Co_3O_4), 0.5 mg of carbon black, with 15 μL Nafion solutions (5 wt%) were dispersed in 1.0 mL ethanol with the assistance of by sonication 10–20 min to form a homogeneous catalyst ink. For kinetic study, 10 μL of the as-prepared catalyst ink was then drop-casted on to a polished mirror-like glassy carbon electrode (5 mm in diameter), and dried in air at room temperature (25 °C). In order to ensure enough samples for physical characterizations of reacted catalysts, we also prepared carbon paper electrodes following the same drop-casting strategy but with relatively larger amount loading of oxide catalysts (7.5 mg/cm^2), for EIS, *operando* Raman spectroscopy, and *in situ* gas chromatography measurements.

Transition metal hydroxides were prepared by electrodeposition at a constant potential of −1.0 V vs. Ag/AgCl for 360 s in 0.1 M $Ni(NO_3)_2$, $Co(NO_3)_2$ and $FeCl_3$ aqueous solutions, respectively. Carbon paper with a deposition area of 1 × 1 cm^2, platinum sheet and saturated Ag/AgCl electrode were used as working electrode, counter electrode and reference electrode, respectively. Before UOR tests, the obtained film catalysts were further activated in 1.0 M KOH solution through continuous CV cycling at a scan rate of 10 mV s-1 in a potential range of 1.1 V_{RHE} to 1.7 V_{RHE}.

Tafel curves were derived from the forward scans of CV curves. Ohmic drops were corrected by subtracting the electrolyte resistance determined by high-frequency AC impedance, where *iR*-corrected potentials are denoted as $E - iR$ (i as the current and R as the electrolyte resistance).

The electrochemical impedance spectra (EIS) measurements were recorded in a frequency range of 0.1 ∼ 100000 Hz with an amplitude of 5 mV. The working electrodes were activated by 10–20 cycles of CV at 20 mV s-1 in 1 M KOH. For each measurement a fresh electrolyte was used to ensure that adsorbates from previous experiments did not influence the result.

2.4. DFT calculations

All first-principles calculations are performed using the Vienna Ab initio Simulation Package (VASP) [34]. The generalized gradient approximation (GGA) of Perdew-Burke-Ernzerhof (PBE) functional was used for describing the electronic exchange and correlation [35]. The projector augmented wave (PAW) method [36]was used to describe the wave function of the interaction between ion and core electrons, while plane waves with 400 eV cutoff energy were extended the Kohn-Sham (KS) wave functions. In geometric optimization, the total energy was converged to 10^{-5} eV, and the Hellmann-Feynman force on each relaxed atom was less than 0.02 eV/Å. Set the vacuum space between two adjacent sheets to at least 15 Å to eliminate interaction between each other. The DFT + U parameter (U value) was set as 5.0, 5.9, 5.3 eV for Fe, Co, Ni, respectively. The long-range interactions (DFT-DF3) are considered as a correction in all the calculations [37]. Spin polarization was included for the correct description of magnetic properties.

3. Results and discussion

3.1. Electrocatalytic activities of UOR and OER

Upon the anodic treatment, urea molecules can be destroyed during the oxidation reaction due to the subtraction of one or more electrons from its structure. However, the exact mechanisms and kinetics of urea decomposition on various electrode materials may differ, largely depending on the electrostatic interactions between the heterogenous structure and urea molecules in electrolyte, as well as the intermediate products formed on catalyst surface, both affecting the reaction pathways and activation energy of rate determining steps (RDS) [38]. In addition, there could be many other factors affecting the overall catalytic performance, including the crystal structure, composition, particle size, morphology and etc. To simplify the study, three powders of metal oxides purchased without further treatment were adopted as model catalysts in this study, including NiO in a rock-salt structure, Co_3O_4 with a spinel structure, and hematite α-Fe_2O_3 powders (Fig. 1). We attempted to make surface chemical composition and structure are the only variable factor in the mechanistic analysis.

To eliminate the potential influence of powder morphology, structure, and other factors, systematic physical characterizations were conducted on these oxides before electrochemical measurements. The crystal structure of these commercial oxide powders was confirmed by powder XRD measurements (Fig. S1). High-resolution TEM (Fig. S2) was employed to analyze their exposed facets which were implemented as model facets in later DFT studies. BET surface area was determined from nitrogen adsorption desorption isotherms (Fig. S3), which is significant for probing the intrinsic catalytic activities of different oxides for UOR. At last, considering that most oxides could inevitably form thin layers of (oxy)hydroxides on their particle surfaces during electrochemical treatment in alkaline media, which may function as real catalytic material, Ni-/Co–/Fe- hydroxides thin films were therefore prepared via a simple electrodeposition method for comparison. As schematically proposed in Fig. 1, the research objective is to

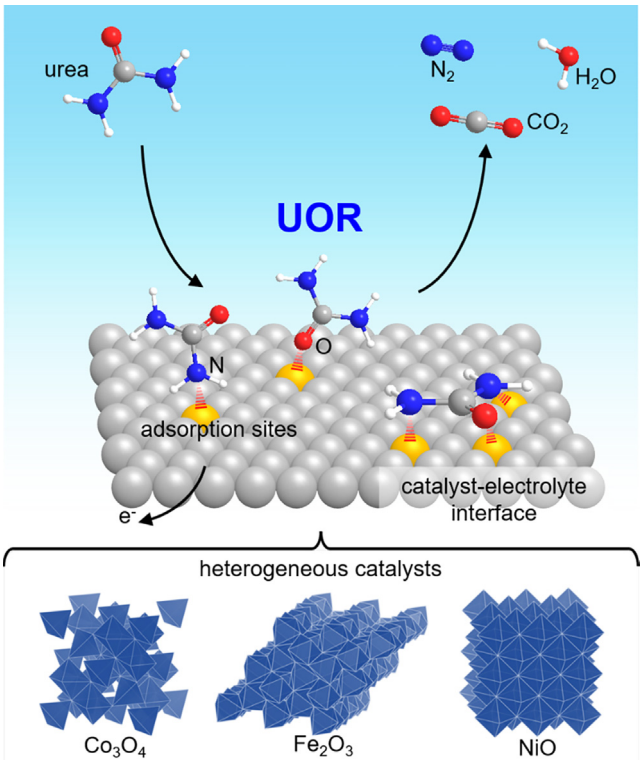

Fig. 1. Schematic illustration of the dynamic electrochemical processes involved during UOR on catalyst surface, including urea adsorption, dissociation, and further electrochemical oxidation. Three transition metal oxides (spinel-type Co_3O_4, hematite α-Fe_2O_3, and rock-salt structured NiO) were selected as model catalysts to investigate the catalytic behaviors and mechanisms of UOR.

establish a more intimate connection between urea decomposition and heterogeneous Ni-/Co–/Fe- based catalyst systems.

The kinetics of OER and UOR on different Ni-/Co–/Fe-oxides and hydroxides was firstly investigated in 1.0 M KOH solution, with and without the addition of 0.33 M urea using glass carbon and carbon paper electrode, respectively. Fig. 2a-2c display the CV curves of these oxides measured in different electrolytes. All catalysts demonstrated modest OER activities in alkaline media, whereas for UOR, the NiO showed a superior catalytic performance than other oxides, with a drastic increase of the anodic current at 1.35 V vs. RHE. In order to better understand the involved redox behaviors on the surface, CV curves were enlarged at the typical capacitance region as shown in Fig. S4a-4c. A pair of reversible redox peaks is observed at 1.35 V vs. RHE for NiO. Interestingly, the catalytic oxidation of urea also occurs concomitantly at the same potential region. With the addition of 0.33 M urea in KOH electrolyte, the anodic current drastically increased in the potential range of 1.35–1.55 V vs. RHE. This phenomenon was explained in many previous studies [29,39]. It's generally considered that Ni^{3+} is the active sites for urea oxidation [33].

When 0.33 M of urea was added to the alkaline electrolyte, the OER performance of the Co_3O_4 catalyst is suppressed at high potentials (Fig. 2b). A reversible redox peak appeared at 1.43 V vs. RHE, which is attributed to the redox of $Co^{3+/4+}$ in alkaline media [40]. Particularly, the Co^{4+} is responsible for the catalytic oxidation of adsorbed water molecules [41]. The catalytic oxidation of urea also occurs at the same potential region, but the associated UOR activity is relatively poor compared to NiO. For Fe_2O_3 catalyst, the addition of urea showed no obvious change in CV curves (Fig. 2c). Furthermore, we didn't observe any reversible redox peaks in Fig. S4c, but there is an increase of the anodic current at potential regions between 1.4 and 1.55 V vs. RHE, indicating that the UOR takes place but is poorly reacted. Beyond this potential, water oxidation seems to be the dominant reaction occurring on catalyst surface.

The corresponding Tafel plots of these CV curves were plotted in Fig. S4d-4f, which revealed more information of the reaction kinetics for three metal oxide catalysts. For both NiO and Co_3O_4, the catalytic UOR seems to be associated with the formation of higher valent metal sites such as Ni^{3+} at 1.32 V vs. RHE and Co^{4+} at 1.36 V vs. RHE, respectively. Since there is no further oxidation of Fe^{3+} on Fe_2O_3, UOR occurs above 1.4 V vs. RHE. In 0.33 M urea solution, the Tafel slopes of NiO (24 mV dec^{-1}) is much lower than that of Co_3O_4 and Fe_2O_3 (127 mV dec^{-1} and 145 mV dec^{-1}, respectively), revealing the higher kinetics for UOR on NiO catalyst. At elevated

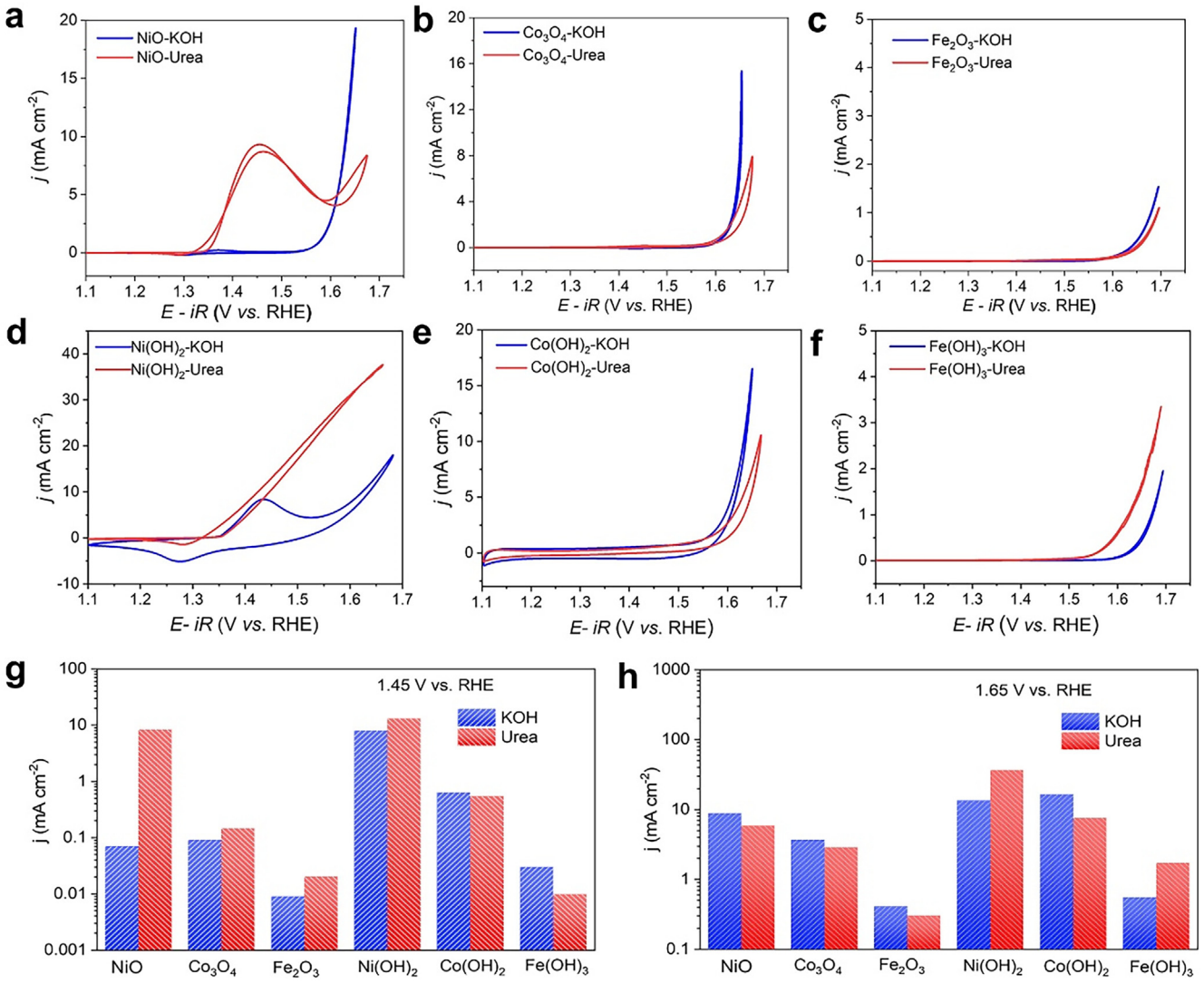

Fig. 2. Electrochemical performance of different transition metal oxides and hydroxides for UOR and OER in 1.0 M KOH solution with and without urea: (a-c) CV curves of commercial NiO, Co_3O_4 and Fe_2O_3 powders as electrocatalysts, (d-f) CV curves of electrodeposited $Ni(OH)_2$, $Co(OH)_2$ and $Fe(OH)_3$ as electrocatalysts. Comparison of the anodic UOR and OER currents at 1.45 V (g) and 1.65 V vs. RHE (h).

potentials OER takes place as a competitive reaction to UOR on catalyst surface. The Tafel slope of NiO is largely increased from 47 mV dec^{-1}in KOH to 234 mV dec^{-1} in KOH solution with urea, suggesting that the surface coverage of reaction intermediates during UOR may block the reactive sites resulting in decreased OER catalytic ability. However, this phenomenon was not observed on Co_3O_4 or Fe_2O_3.

As mentioned above, for comparison, we also prepared transition metal hydroxides of $Ni(OH)_2$, $Co(OH)_2$ and $Fe(OH)_3$ by electrodeposition method. As shown in Fig. 2d-2f, the obtained hydroxides demonstrated similar electrochemical performance in both OER and UOR. Particularly, the $Ni(OH)_2$ deposit exhibited unique catalytic activity in urea-containing alkaline solution. Especially, the UOR starts at a very low potential of ~ 1.4 V vs. RHE, which is also associated with the electrochemical oxidation of Ni sites from Ni^{2+} to Ni^{3+}. Comparing to NiO, we didn't observe the decrease of anodic current at elevated potentials, e.g., 1.6 V vs. RHE. This phenomenon reflected the dynamic equilibrium occurring on catalyst interfaces following the electrochemical-chemical reaction mechanism. The electrochemically oxidized Ni^{3+} can be chemically reduced by adsorbed urea molecules to Ni^{2+}, which were continuously oxidized to Ni^{3+}. Owing to the limited active sites of NiO, and the amount of $Ni^{2+/3+}$ cationic redox centers is much smaller than that in $Ni(OH)_2$. Upon increasing electrode potentials, the electro-oxidation of Ni^{3+} and subsequent chemical reduction by urea reaches a dynamic equilibrium on the catalyst-electrolyte interfaces. The oxide surface is quickly covered by intermediate products, resulting in a decrease of the anodic current. Benefiting from the enriched Ni sites in the electrodeposited $Ni(OH)_2$, this dynamic equilibrium cannot be reached due to sufficient removal of urea from the catalyst surface. In contrary, $Co(OH)_2$ didn't display any catalytic activity towards UOR (Fig. 1e). Interestingly, $Fe(OH)_3$ can oxidize urea at higher potentials at 1.55 V vs. RHE, however, the activity is much poorer than that of $Ni(OH)_2$.

Fi g. 2 g-2 h further summarized the anodic currents of transition metal oxides and hydroxides obtained at different potentials. At a low potential of 1.45 V vs. RHE, the NiO exhibited a unique catalytic performance towards UOR among all catalysts. However, its corresponding hydroxide form, $Ni(OH)_2$, didn't display any promising activity in urea-containing KOH solution. This observation is out of expectation, since $Ni(OH)_2$ clearly possesses more exposed Ni sites than NiO on surface. It's therefore hypothesized that the charge-transfer resistance at the interfaces may also strongly influence the kinetics of chemical reactions between Ni^{3+} and urea molecules at low potentials. Both Co_3O_4 and $Co(OH)_2$ demonstrated negligible activities towards UOR. Particularly, the currents were even reduced at 1.65 V vs. RHE, suggesting that the presence or adsorption of urea molecules on cobalt catalyst surface may block the active sites for OER. When it comes to Fe_2O_3 and $Fe(OH)_3$, there is little increase of the current density of UOR at 1.65 V vs. RHE, indicating their catalytic properties function at higher potentials. Finally, it's worth to mention that the current densities are normalized by geometric surface area of the electrode. To reflect the intrinsic activity, the anodic currents were also normalized by BET surface area. As shown in Fig. S5, the NiO still demonstrated the unique highest UOR activities.

3.2. In situ gas chromatography measurement for H_2 production

In order to further compare the differences in the activity of the three catalysts in electrocatalytic oxidation of urea, *in situ* gas chromatography was conducted to examine the practical yield of H_2 during the electrochemical operation in 1 M KOH with or without 0.33 M urea solution. Carbon paper electrodes were prepared as work electrode base for *in situ* gas chromatography, a piece of Pt plate is used as the cathode to assist HER. As shown in Fig. 3, at a low working potential (1.45 V vs. RHE) and in the absence of urea, H_2 cannot be detected by the gas chromatography from all three catalyst systems. After adding 0.33 M urea into the anodic electrolyte, over 3000 ppm of H_2 can be detected from the system using NiO catalyst as the anode, which is 5 times that of the Co_3O_4 catalyst system (~600 ppm). Results clearly proved the superior ability of NiO for assisting hydrogen production by urea electrolysis with lower energy input. When the electrode potential raised to 1.65 V vs. RHE, H_2 was detected on all the three catalyst systems. It's noticed that the amount of H_2 produced in both Co_3O_4 and Fe_2O_3 catalyst systems show less affection by the addition of urea into the KOH electrolyte. Thus, results of the *in-situ* gas chromatography measurements suggested that the NiO-based catalyst could play a unique role in practical urea-assisted H_2 production technology.

3.3. EIS study of UOR

Rather than DC technology, AC technology can be used in EIS to provide more dynamic and electrode interface information in a wider frequency range [42]. Accordingly, the electrochemical properties of these three oxides towards OER and UOR were further evaluated by EIS.

Fig. 4 compares the Nyquist plots and Bode plots of NiO in KOH solution with and without urea. In order to depict the dynamic evolution of involved reactions, the applied potential of EIS is stepwise increased from 1.35 to 1.65 V vs. RHE. In a pure KOH solution,

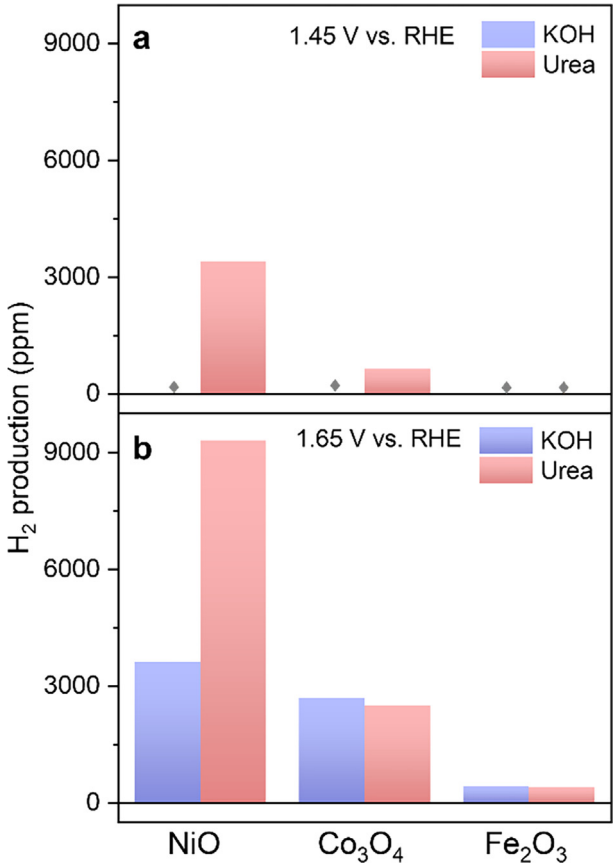

Fig. 3. H_2 production detected by *in situ* gas chromatography in different catalyst systems (using Pt plate as cathode and NiO, Co_3O_4, Fe_2O_3 as the anode) by holding electrode potential at 1.45 and 1.65 V vs. RHE for 10 mins in 1.0 M KOH solution with or without 0.33 M urea. (Grey diamond markers indicate negligible detection of H_2 gas by GC.).

a semi-circle is observed in the Nyquist plot at 1.60 V vs. RHE, which is an indication for triggering the OER electrochemical process on electrode surface. In the presence of 0.33 M Urea (Fig. 4b), the semi-circle appears at a much lower potential (1.40 V vs. RHE). The impedance measured at 1.4 V on NiO catalyst are significantly different in KOH with and without Urea. We consider this phenomenon as a strong indication as the start point for urea electrolysis on NiO surface. The reduced size of semicircle of impedance spectra reflected the small charge transfer resistance, which is directly associated to the fast reaction kinetics of the urea electrolysis occurring on solid–liquid interfaces. The size of the semi-circle continuously decreased at higher potentials of 1.55 V vs. RHE. However, as the voltage increase, a reverse circuit with negative real part impedance at 1.65 V vs. RHE was observed. It has been reported that impedance changes are often encountered during electrooxidation of methanol and ethanol on Pt-based catalysts. For example, Hsing et al. [43] verified through theoretical calculation and experimental results that CO, the intermediate produced in electrocatalytic methanol oxidation, would strongly adsorb on the catalyst surface. Once the electrooxidation intermediate process becomes a rate-determining step or its rate is comparable to that of the dehydrogenation process, the impedance diagram will be reversed from the first quadrant to the second, or extended to the third and fourth quadrants. This phenomenon observed at 1.65 V vs. RHE is also consistent with the results of CV in Fig. 2a, which can be well explained by the dynamic point of view on catalyst-electrolyte interfaces. The reversal of resistance in EIS originates from the surface state quantity X, which represents the late desorption of intermediate products formed on the electrode surface, or the formation of passivation film covered on the electrode surface. Generally, in electrochemical reaction, the current–voltage relationship satisfies the dynamic formula of B-V equation. Current I is a function of voltage E and surface state quantity X. Under the disturbance of △E, the function of current total differential can be derived as [44,45]:

$$\Delta I = (\frac{\partial I}{\partial E})\Delta E + (\frac{\partial I}{\partial X})\Delta X$$

The impedance can be written as:.$Z = R_{ct} + \frac{\frac{R_{ct}{}^2|B|}{a-R_{ct}|B|}}{1+j\omega\frac{1}{a-|B|R_{ct}}}$

B represents the product of the partial differential of current to voltage and the change rate of surface state quantity X to the partial differential of X, a represents change rate of surface state quantity X to the partial differential of E.

When $B < 0$, $a - R_{ct}|B| < 0$, the equivalent resistance of impedance is negative, which makes the impedance diagram reversed. Therefore, we speculate that at 1.65 V vs. RHE, the surface of NiO is fully covered by intermediate products, which block the reactive sites for further reaction. Overall, the abnormal phenomenon at 1.65 V vs. RHE observed on NiO shows that the electrochemical reaction is jointly controlled by kinetics, diffusion, adsorption and desorption. It is confirmed that the adsorption and desorption of the intermediate product CO_2 affects the catalytic performance of NiO material.

In the corresponding Bode plot for UOR, a peak is observed at a low frequency of $10^{-0.01}$ Hz at 1.40 V vs. RHE, indicating that there

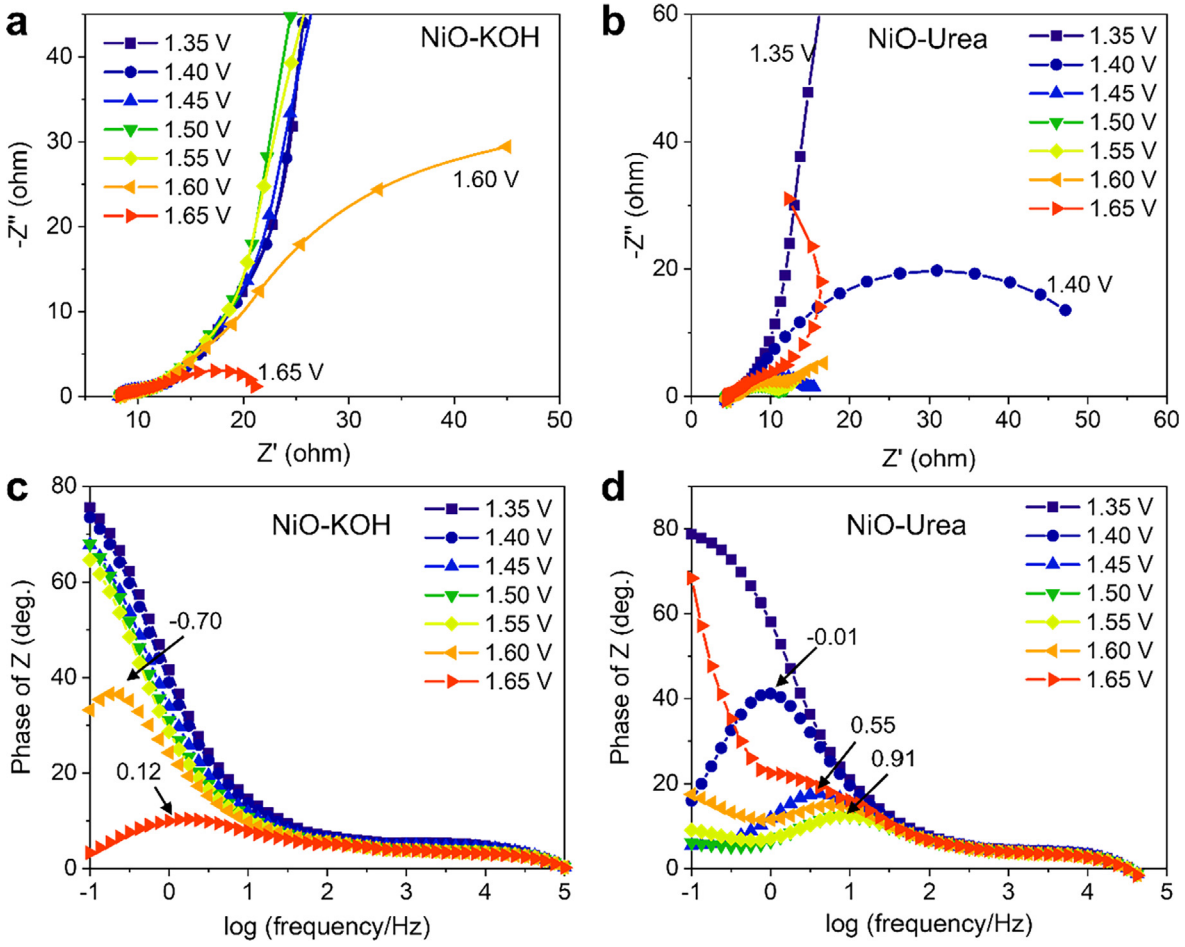

Fig. 4. Evolution of EIS spectra using NiO as electrocatalyst with increasing applied potentials in 1 M KOH (a, c) and 1 M KOH with 0.33 M Urea (b, d).

is a charge-transfer process involved on NiO surface at this potential. Moreover, it's noted that the peak center is quickly shifting to $10^{0.55}$ Hz at 1.45 V vs. RHE, and further to higher frequencies ($10^{0.91}$ Hz) at elevated potentials. The peak position reflected the time domain of the charge-transfer process, which is associated to the kinetics of the electrochemical reactions. Clearly, comparing to the OER process, the kinetics of urea oxidation on Ni surface is much faster.

EIS studies were also carried out on Co_3O_4 and Fe_2O_3 electrodes. In Fig. 5a, for the Co_3O_4 catalyst in KOH solution, all EIS spectra in the potential range from 1.35 V to 1.60 V vs. RHE show diagonal lines with no semi-circles formed, which is a typical symptom of electric double layer capacitive behavior with large Warburg diffusion resistance at these potentials. Up to 1.65 V vs. RHE, the Co_3O_4 starts to catalyze water oxidation. Comparing to the EIS spectra obtained in urea-contained KOH solution, the involved diffusion resistance decreased slightly. At 1.60 V vs. RHE, a semi-circle is observed indicating the catalytic oxidation of both urea and water. However, based on the size the semi-circle, a relatively large charge-transfer resistance of ~ 30 Ω is expected. Similar evolution trend of the EIS spectra is also observed on Fe_2O_3 electrode as shown in Fig. 6. In addition, the peak positions in the corresponding Bode plot for Co_3O_4 and Fe_2O_3 at 1.45 V vs. RHE is estimated to be $10^{-0.63}$ and $10^{-0.17}$ Hz, respectively, both are ten times smaller than that of NiO ($f = 10^{0.55}$ Hz).

3.4. Electrochemical operando Raman spectroscopy

So far, we evaluated the electrochemical properties of these three oxide catalysts for OER and UOR by CV and EIS, and confirmed the superior performance of NiO towards UOR. The different electrochemical behaviors of three typical catalysts during UOR proved that the reaction was an inner sphere reaction, which strongly depended on the formation of surface reactive intermediates. However, using these classical electrochemical methods can only provide some indirect and incomplete information on reaction kinetics, which is still difficult to depict the dynamic electrochemical processes involved on electrode surface.

Therefore, a combination of electrochemical measurement and *operando* Raman spectroscopy was developed to monitor the dynamic formation of reaction intermediates on the electrocatalyst surface [46]. In order to better understand the unique catalytic activity of NiO for catalysis of urea oxidation, we further carried out *operando* Raman spectroscopy study (Fig. 7). It's expected that the analysis can provide more valuable information to help us figure out the underlying mechanism.

Fig. 7 shows the evolutions of Raman spectra for NiO, Co_3O_4, and Fe_2O_3 catalysts in KOH solution with and without addition of urea. The potential applied on the catalyst electrodes is stepwise increased from 1.25 to 1.65 V vs. RHE with an interval of 50 mV per spectroscopy. The most interested sample is NiO as shown in

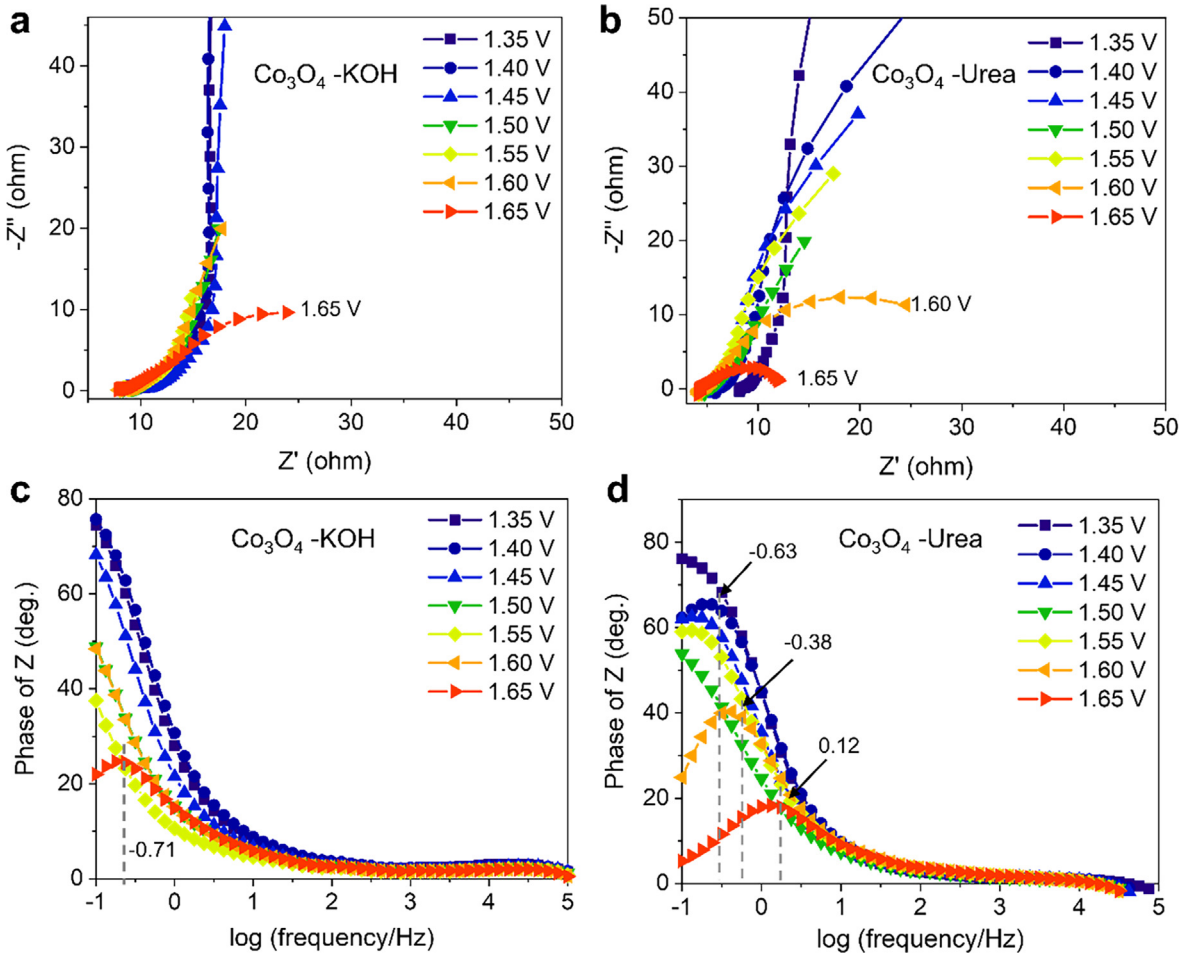

Fig. 5. Evolution of EIS spectra using Co_3O_4 as electrocatalyst with increasing applied potentials in 1 M KOH (a, c) and 1 M KOH with 0.33 M Urea (b, d).

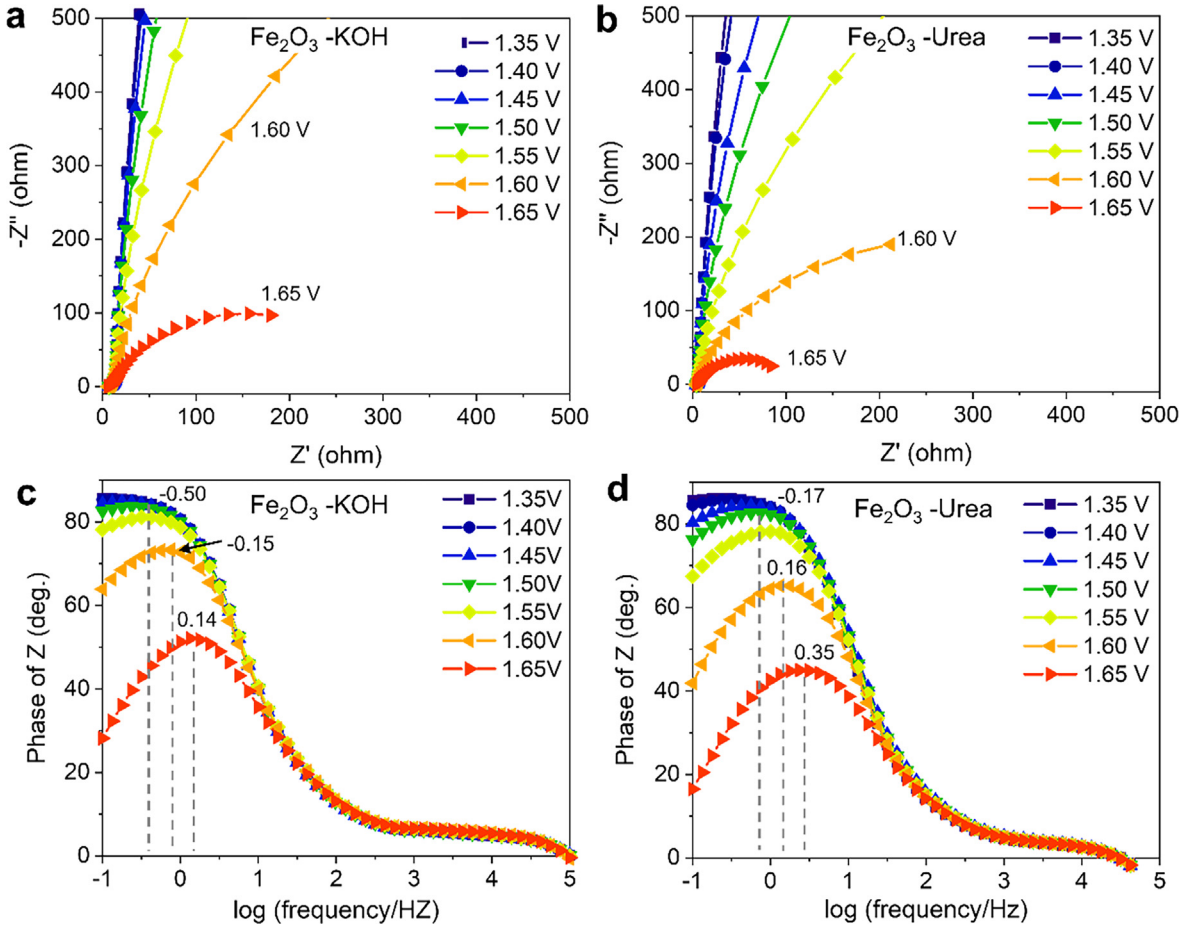

Fig. 6. Evolution of EIS spectra using Fe_2O_3 as electrocatalyst with increasing applied potentials in 1 M KOH (a, c) and 1 M KOH with 0.33 M Urea (b, d).

Fig. 7a for OER and Fig. 7d for UOR. Two peaks centered at 476 cm^{-1} and 556 cm^{-1} appeared above 1.45 V vs. RHE in in both KOH and KOH/urea electrolytes. Accordingly, these two peaks can be ascribed to Ni-O bending and stretching vibration characteristics of NiOOH, which is strong indication for the formation of a thin layer of NiOOH on NiO surface [47,48]. At the meantime, another broad signal detected at 1003 cm^{-1} representing the symmetric C—N stretching vibration in urea disappeared concomitantly, indicating that urea was electrochemically oxidized by NiOOH catalyst. It's thereby concluded that the formation of NiOOH is the key material for triggering the high catalytic performance for urea electrooxidation.

The evolution of Raman peaks of Co_3O_4 were carefully monitored and the results are shown in Fig. 7b and 7e. The characteristic peaks at 483, 525 and 690 cm^{-1} are matching well with the original Co_3O_4 [49]. The Raman bands located at 483 and 525 cm^{-1} have the Co-O symmetric E_g and asymmetric F_{2g} bending, respectively. The strong band at about 690 cm^{-1} is assigned to the A_g species of Co-O symmetric stretching. The well-maintained Raman peaks reflected the good structural integrity of Co_3O_4 in alkaline solution for OER and UOR. It is interesting to note that no obvious Raman features of CoOOH have been observed. The most possible reason is that the Co ions in solid spinel Co_3O_4 are strongly bonded with O anions [50].

The same phenomenon also observed on Fe_2O_3 electrode in Fig. 7c and 7f. The vibration bands at 225 cm^{-1} is A_{1g} mode and 293, 412, 613 and 1322 cm^{-1} have four E_g mode, which can be assigned to the characteristics of Fe_2O_3 crystal structure [51]. Upon electrochemical oxidation, we didn't observe any shifts of these bands. Overall, from our current results, it's difficult to conclude that there is an involvement of oxyhydroxide species on the surface of Co_3O_4 or Fe_2O_3 during UOR.

3.5. Surface adsorption behavior of urea molecules

As discussed above, we identified the key intermediates NiOOH formed on NiO surface by *operando* Raman spectroscopy, which may be responsible for the high catalytic activity observed during UOR. Since electrochemical reactions normally take place on catalyst surface, the surface electronic structure of the catalyst, including the adsorption barrier of the intermediate and the overall charge transfer can significantly influence the dynamics of the process. Therefore, we further conducted DFT calculations to depict the adsorption process of urea molecules on various catalyst surfaces. This insight into the solid – liquid interface is essential for understanding the thermodynamics of catalytic reactions.

For simplicity, the [200] facet of NiO, [220] of Co_3O_4, [104] of Fe_2O_3, [001] of NiOOH, [001] of CoOOH and [010] of FeOOH were selected for calculation. Combined with XRD patterns (Fig. S4), crystal facets of oxides were identified from TEM observations which were found largely exposed on oxide samples used in our measurements (Fig. S5). Based on the DFT calculations, the most stable coordination of urea molecule on these facets are identified and plotted in Fig. 8a-f. On the [104] facet of Fe_2O_3, O atom in urea interacted with exposed Fe sites, while the protons in $–NH_2$ groups interacted with surface lattice oxygens. Similarly, O atoms are

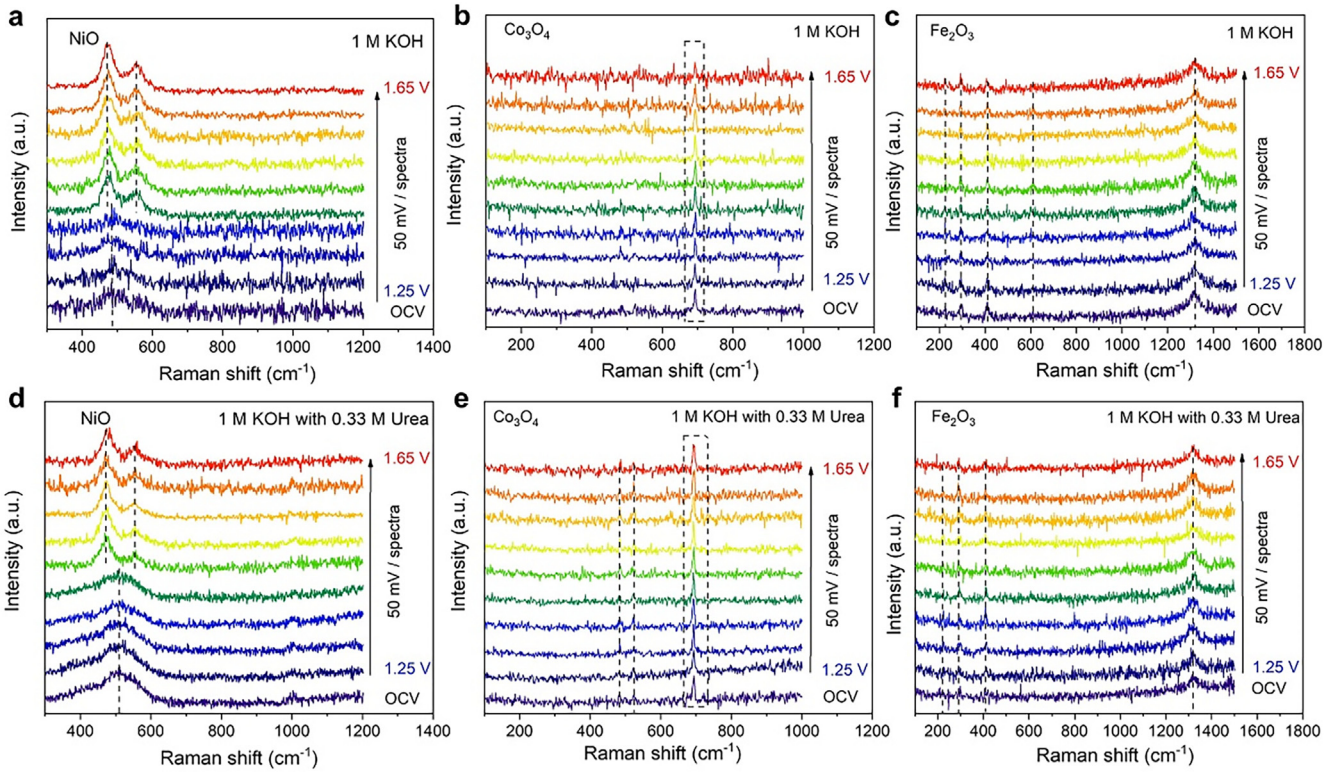

Fig. 7. *Operando* Raman spectroscopy of different metal oxides for OER and UOR operation.

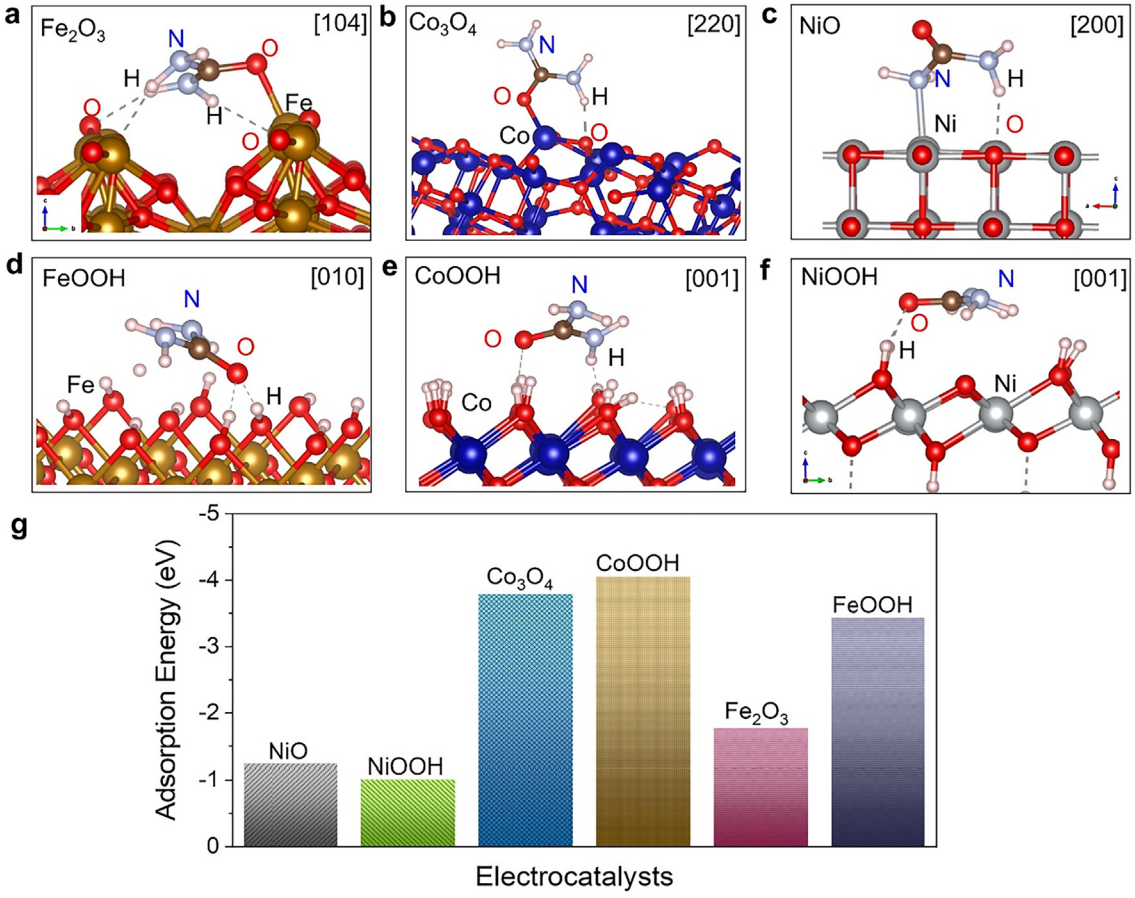

Fig. 8. Urea molecule adsorptions on selective facet of (a) Fe_2O_3, (b) Co_3O_4, (c) NiO, and (d)FeOOH, (e)CoOOH, (f) NiOOH, (g) The calculated adsorption energies of urea molecule on different catalyst surface.

strongly interacted on the [220] facet of Co_3O_4, leading to a bridge coordination of the structure. The preferential interaction between N atoms in the two-NH_2 groups with Ni leads to a *N*-coordinated bridge structure on NiO surface. The adsorption behavior on M−OOH is significantly different from other oxides.

Urea molecule adsorbed specifically on the [001] facet of CoOOH with hydrogen bonds dominated by O and H atoms. [010] facet of FeOOH with hydrogen bonds dominated with O atom, and the [001] facet of NiOOH with hydrogen bonds dominated with O atom at the interactions. Based on the literature, most transition metal atoms are found to interact with either the nitrogen or oxygen atom of the urea molecule as observed in many transition metal-urea complexes of Pd, Pt, Cr, Fe, Zn, and Cu [52].

The corresponding adsorption energy in these stabilized modes is compared in Fig. 8g. It's noted that Co_3O_4 has a strong electronic interaction with urea molecule, with the thermodynamic value up to −3.8 eV. Based on the Sabastian principle that the catalyzed molecules/intermediate should be moderately adsorbed on reactive sites for achieving best performance. Such a strong adsorption is probably not suitable for catalysis. As a result, the adsorption energy of urea molecule on different catalyst surface is indeed largely influenced by the interactions, resulting in different space configuration and coordination structures.

The adsorption strength reflects the thermodynamic energy barriers to overcome. It has been widely discussed and employed as an activity descriptor in evaluating the OER catalysts. Tao et al. proved the oxygen intermediates generated at OER electrochemical reaction interfaces of transition metal oxides, revealed the bond formation energies of intermediates that control OER kinetics of various catalysts, and the unique configurations of valence electrons in oxygen intermediates [53]. Subbaraman et al. reported that the OER activity of metal hydroxides (Ni, Co and Fe) follows the order of Ni > Co > Fe, and the performance of OER was related with the strength of OH_{ad}-M^{n+} [54]. Recently, the adsorption energy of urea molecules has also been intensively discussed in UOR. For example, Schranck et al. demonstrated a strategy to disrupt the interaction between urea and catalyst sites in the Stern layer by introducing other molecules or ions in the electrolyte, such as phosphate ions, which would effectively inhibit the UOR performance [55]. However, results of our DFT calculations suggested that extra care should be taken when employing the adsorption energy as activity descriptor for UOR, since all NiO, NiOOH and Fe_2O_3 demonstrated similar values for adsorption energies of urea molecules on their surfaces.

Indeed, the electrochemical processes occurring on the solid–liquid interfaces during urea electro-oxidation is very complicated, because 6 consecutive PCETs could be involved in the presence of OH^- groups. The complete decomposition of urea molecules involves the specific adsorption at reactive sites, stepwise deprotonation by OH^-, and N—N bond formation, which are intrinsically regulated by interactions between urea and the solid oxide catalysts. It's therefore anticipated that the initial coordination and configuration of adsorbed urea molecules should impose large influences on the thermodynamics and kinetics of the following steps. In addition to urea molecules, the adsorption of hydroxide groups is another competitive process involved on catalyst surface, which not only participates in the following deprotonation process but also further affects the urea-catalyst interactions on catalyst surface [56]. It's reported that due to the presence of the hydroxide in NiOOH, a bridging coordination was proposed for the adsorption of urea on NiOOH surface [56]. This is considered similar to urease oxidation of urea where the Ni atoms of urease interact with N and O of urea, while the bridging oxygen of urease interacts with the carbon atom of urea [57].

4. Conclusions

In summary, we employed three transition metal oxides as model catalysts to investigate the fundamental electrocatalytic behaviors towards OER and UOR in alkaline media. Both CV and EIS studies proved that all catalysts can catalyze the oxidation of urea with a rank of NiO > Co_3O_4 > Fe_2O_3. Among these oxides, NiO demonstrated an abnormal high catalytic activity towards UOR. Elevated working potentials higher than 1.6 V vs. RHE would inevitably introduce more water oxidation on these catalysts. *Operando* electrochemical Raman spectroscopy was employed to understand the surface structure evolution, and capture the intermediates formed during UOR. As a result, we identified the formation of Ni (oxy)hydroxide on NiO surface, which should be responsible for the high catalytic activity of UOR. On the other hands, neither Co_3O_4 or Fe_2O_3 leads to the formation of such (oxy)hydroxide layers during UOR in our study. DFT calculations on the adsorption energy of urea molecules on NiO, Co_3O_4, Fe_2O_3, NiOOH, CoOOH and FeOOH, further revealed that there could be a large dependence on the regulations of the space configuration of adsorbed urea molecules. In other words, the simple calculation by adsorption energy may not be a good activity descriptor for UOR, although this has been widely used in evaluating the catalyst activity in many previous literatures. Overall, results of this work provide mechanistic insights into the competitive oxidative processes on the solid–liquid interface during urea oxidation. With continued development and research focused on improving the activity and selectivity, electrolytic urea oxidation represents an attractive strategy for sustainably treating source-separated urine.

CRediT authorship contribution statement

Jianhua Ge: Writing – original draft, Writing – review & editing. **Zhongfei Liu:** Writing – review & editing. **Minghui Guan:** . **Juner Kuang:** Visualization, Validation. **Yuhua Xiao:** Writing – review & editing. **Yang Yang:** Data curation, Software. **Chi Him Tsang:** Writing – review & editing, Supervision. **Xiao ying Lu:** Resources, Writing – review & editing, Supervision, Funding acquisition. **Chunzhen Yang:** Resources, Writing – review & editing, Supervision, Funding acquisition.

Declaration of Competing Interest

The authors declare that they have no known competing financial interests or personal relationships that could have appeared to influence the work reported in this paper.

Acknowledgements

This work is financially supported by the National Natural Science Foundation of China (Projects No. 21972172), Hong Kong Environment and Conservation Fund (No.: 39/2019) and Hong Kong Competitive Research Funding Schemes for the Local Self-financing Degree Sector Faculty Development Scheme (No.: UGC/FDS25/E06/19).

Appendix A. Supplementary material

Supplementary data to this article can be found online at https://doi.org/10.1016/j.jcis.2022.03.152.

References

[1] X. Xiao, L. Yang, W. Sun, Y. Chen, H. Yu, K. Li, B. Jia, L. Zhang, T. Ma, Electrocatalytic water splitting: from harsh and mild conditions to natural seawater, Small 18 (2021) 2105830.

[2] M. Gong, Y. Li, H. Wang, Y. Liang, J.Z. Wu, J. Zhou, J. Wang, T. Regier, F. Wei, H. Dai, An advanced Ni–Fe layered double hydroxide electrocatalyst for water oxidation, J. Am. Chem. Soc. 135 (2013) 8452–8455.
[3] R.M. Choueiri, S.W. Tatarchuk, A. Klinkova, L.D. Chen, Mechanism of ammonia oxidation to dinitrogen, nitrite, and nitrate on β-$Ni(OH)_2$ from first-principles simulations, Electrochem. Sci. Adv. (2021) 2100142.
[4] V. Rosca, M.T.M. Koper, Electrocatalytic oxidation of hydrazine on platinum electrodes in alkaline solutions, Electrochimi. Acta 53 (2008) 5199–5205.
[5] R.G.C.S. dos Reis, F. Colmati, Electrochemical alcohol oxidation: a comparative study of the behavior of methanol, ethanol, propanol, and butanol on carbon-supported PtSn, PtCu, and Pt nanoparticles, J. Solid State Electrochem. 20 (2016) 2559–2567.
[6] M. Baghayeri, A. Amiri, A. Motamedifar, Investigation about electrocatalytic oxidation of glucose on loaded Ag nanoparticles on functionalized carbon nanotubes, Ionics 22 (2016) 1709–1717.
[7] W. Xu, D. Du, R. Lan, J. Humphreys, Z. Wu, S. Tao, Highly active Ni-Fe double hydroxides as anode catalysts for electrooxidation of urea, New J. Chem. 41 (2017) 4190–4196.
[8] B. Zhu, Z. Liang, R. Zou, Designing advanced catalysts for energy conversion based on urea oxidation reaction, Small 16 (2020) 1906133.
[9] J. Ge, Y. Lai, M. Guan, Y. Xiao, J. Kuang, C. Yang, Nickel borate with a 3D hierarchical structure as a robust and efficient electrocatalyst for urea oxidation, Environ. Sci.: Nano 8 (2021) 1326–1335.
[10] V. Amstutz, A. Katsaounis, A. Kapalka, C. Comninellis, K.M. Udert, Effects of carbonate on the electrolytic removal of ammonia and urea from urine with thermally prepared IrO_2 electrodes, J. Appl. Electrochem. 42 (2012) 787–795.
[11] R.L. King, G.G. Botte, Investigation of multi-metal catalysts for stable hydrogen production via urea electrolysis, J. Power Sources 196 (2011) 9579–9584.
[12] W. Simka, J. Piotrowski, G. Nawrat, Influence of anode material on electrochemical decomposition of urea, Electrochimi. Acta 52 (2007) 5696–5703.
[13] D. Wang, G.G. Botte, In situ X-ray diffraction Study of urea electrolysis on nickel catalysts, ECS Electrochem. Lett. 3 (9) (2014) H29–H32.
[14] D. Wang, W. Yan, S.H. Vijapur, G.G. Botte, Electrochemically reduced graphene oxide-nickel nanocomposites for urea electrolysis, Electrochimi. Acta 89 (2013) 732–736.
[15] D. Wang, S.H. Vijapur, Y. Wang, G.G. Botte, NiCo2O4 nanosheets grown on current collectors as binder-free electrodes for hydrogen production via urea electrolysis, Int. J. Hydrogen Energy 42 (2017) 3987–3993.
[16] Y. Tong, P. Chen, M. Zhang, T. Zhou, L. Zhang, W. Chu, C. Wu, Y.i. Xie, Oxygen vacancies confined in nickel molybdenum oxide porous nanosheets for promoted electrocatalytic urea oxidation, ACS Catal. 8 (1) (2018) 1–7.
[17] X. Zhuo, W. Jiang, G. Qian, J. Chen, T. Yu, L. Luo, L. Lu, Y. Chen, S. Yin, Ni_3S_2/Ni heterostructure nanobelt arrays as bifunctional catalysts for urea-rich wastewater degradation, ACS Appl. Mater. Interfaces 13 (30) (2021) 35709–35718.
[18] J. Liu, Y. Wang, Y. Liao, C. Wu, Y. Yan, H. Xie, Y. Chen, Heterostructured Ni_3S_2-Ni_3P/NF as a bifunctional catalyst for overall urea-water electrolysis for hydrogen generation, ACS Appl. Mater. Interfaces 13 (23) (2021) 26948–26959.
[19] N. Kakati, G. Li, P.-Y. Chuang, Insights into the Ni/C-based thin-film catalyst layer design for urea oxidation reaction in a three-electrode system, ACS Appl. Energy Mater. 4 (4) (2021) 4224–4233.
[20] H. Osgood, S.V. Devaguptapu, H. Xu, J. Cho, G. Wu, Transition metal (Fe Co, Ni, and Mn) oxides for oxygen reduction and evolution bifunctional catalysts in alkaline media, Nano Today 11 (5) (2016) 601–625.
[21] L. Han, S. Dong, E. Wang, Transition-metal (Co, Ni, and Fe)-based electrocatalysts for the water oxidation reaction, Adv. Mater. 28 (42) (2016) 9266–9291.
[22] F. Franco, C. Rettenmaier, H.S. Jeon, B. Roldan Cuenya, Transition metal-based catalysts for the electrochemical CO_2 reduction: from atoms and molecules to nanostructured materials, Chem. Soc. Rev. 49 (19) (2020) 6884–6946.
[23] Y. Tong, L.u. Chen, P.J. Dyson, Z. Fei, Boosting hydrogen production via urea electrolysis on an amorphous nickel phosphide/graphene hybrid structure, J. Mater. Sci. 56 (31) (2021) 17709–17720.
[24] J. Xie, W. Liu, X. Zhang, Y. Guo, L.i. Gao, F. Lei, B.o. Tang, Y.i. Xie, Constructing hierarchical wire-on-sheet nanoarrays in phase-regulated cerium-doped nickel hydroxide for promoted urea electro-oxidation, ACS Mater. Lett. 1 (1) (2019) 103–110.
[25] X. Xu, P. Du, T. Guo, B. Zhao, H. Wang, M. Huang, In situ grown Ni phosphate@$Ni_{12}P_5$ nanorod arrays as a unique core-shell architecture:competitive bifunctional electrocatalysts for urea electrolysis at large current densities, ACS Sustain. Chem. Eng. 8 (19) (2020) 7463–7471.
[26] M.A. Pérez-Sosa, E. Ramírez-Meneses, A. Manzo-Robledo, J. Mateos-Santiago, M.A. Hernández-Pérez, V. Garibay-Febles, L. Lartundo-Rojas, G. Zacahua-Tlacuatl, Enhanced performance of urea electro-oxidation in alkaline media on PtPdNi/C, PtNi/C, and Ni/C catalysts synthesized by one-pot reaction from organometallic precursors, Int. J. Hydrogen Energy 46 (41) (2021) 21419–21432.
[27] J. Xie, L.i. Gao, S. Cao, W. Liu, F. Lei, P. Hao, X. Xia, B.o. Tang, Copper-incorporated hierarchical wire-on-sheet α-$Ni(OH)_2$ nanoarrays as robust trifunctional catalysts for synergistic hydrogen generation and urea oxidation, J. Mater. Chem. 7 (22) (2019) 13577–13584.
[28] Z.-Y. Yu, C.-C. Lang, M.-R. Gao, Y.u. Chen, Q.-Q. Fu, Y.u. Duan, S.-H. Yu, Ni-Mo-O nanorod-derived composite catalysts for efficient alkaline water-to-hydrogen conversion via urea electrolysis, Energy Environ. Sci. 11 (7) (2018) 1890–1897.
[29] W. Yan, D. Wang, L.A. Diaz, G.G. Botte, Nickel nanowires as effective catalysts for urea electro-oxidation, Electrochimi. Acta 134 (2014) 266–271.
[30] D. Wang, S. Liu, Q. Gan, J. Tian, T.T. Isimjan, X. Yang, Two-dimensional nickel hydroxide nanosheets with high-content of nickel(III) species towards superior urea electro-oxidation, J. Electroanal. Chem. 829 (2018) 81–87.
[31] X. Zhu, X. Dou, J. Dai, X. An, Y. Guo, L. Zhang, S. Tao, J. Zhao, W. Chu, X.C. Zeng, C. Wu, Y. Xie, Metallic nickel hydroxide nanosheets give superior electrocatalytic oxidation of urea for fuel cells, Angew. Chem. 55 (2016) 12465–12469.
[32] P. Basumatary, D. Konwar, Y.S. Yoon, A novel Ni Cu/ZnO@MWCNT anode employed in urea fuel cell to attain superior performances, Electrochimi. Acta 261 (2018) 78–85.
[33] V. Vedharathinam, G.G. Botte, Understanding the electro-catalytic oxidation mechanism of urea on nickel electrodes in alkaline medium, Electrochimi. Acta 81 (2012) 292–300.
[34] F.J. Kresse G, Efficient iterative schemes forab initiotot al-energy calculations using a plane-wave basis set, Phys. Rev. B, 54 (1996) 11169–11186.
[35] K.B. John, P. Perdew, M. Ernzerhof, Generalized gradient approximation made simple, Phys. Rev. Lett. 77 (1996) 3865–3868.
[36] G. Kresse, D. Joubert, From ultrasoft pseudopotentials to the projector augmented-wave method, Phys. Rev. B 59 (3) (1999) 1758–1775.
[37] S. Grimme, J. Antony, S. Ehrlich, H. Krieg, A consistent and accurate ab initio parametrization of density functional dispersion correction (DFT-D) for the 94 elements H-Pu, J. Chem. Phys. 132 (15) (2010) 154104.
[38] B. Zhu, Z. Liang, R. Zou, Designing advanced catalysts for energy conversion based on urea oxidation reaction, Small 16 (7) (2020) 1906133.
[39] V. Vedharathinam, G.G. Botte, Direct evidence of the mechanism for the electro-oxidation of urea on $Ni(OH)_2$ catalyst in alkaline medium, Electrochim. Acta 108 (2013) 660–665.
[40] M.F. Fink, J. Eckhardt, P. Khadke, T. Gerdes, C. Roth, Bifunctional α-MnO_2 and Co_3O_4 catalyst for oxygen electrocatalysis in alkaline solution, ChemElectroChem 7 (23) (2020) 4822–4836.
[41] Z. Chen, C.X. Kronawitter, B.E. Koel, Facet-dependent activity and stability of Co_3O_4 nanocrystals towards the oxygen evolution reaction, Phys. Chem. Chem. Phys. 17 (2015) 29387–29393.
[42] I.M.A. Mohamed, P. Kanagaraj, A.S. Yasin, W. Iqbal, C. Liu, Electrochemical impedance investigation of urea oxidation in alkaline media based on electrospun nanofibers towards the technology of direct-urea fuel cells, J. Alloys Compd. 816 (2020) 152513.
[43] I.-M. Hsing, X. Wang, Y.-J. Leng, Electrochemical impedance studies of methanol electro-oxidation on Pt/C thin film electrode, J. Electrochem. Soc. 149 (5) (2002) A615.
[44] C.N. Cao, On the impedance plane displays for irreversible electrode reactions based on the stability conditions of the steady-state—I. One state variable besides electrode potential - ScienceDirect, Electrochimi. Acta 35 (1990) 831–836.
[45] C.N. Cao, On the impedance plane displays for irreversible electrode reactions based on the stability conditions of the steady-state—II. Two state variables besides electrode potential, Electrochimi. Acta 35 (1990) 837–844.
[46] B.S. Yeo, A.T. Bell, In situ raman study of nickel oxide and gold-supported nickel oxide catalysts for the electrochemical evolution of oxygen, J. Phys. Chem. C 116 (2012) 8394–8400.
[47] J. Huang, Y. Li, Y. Zhang, G. Rao, C. Wu, Y. Hu, X. Wang, R. Lu, Y. Li, J. Xiong, Identification of key reversible intermediates in self-reconstructed nickel-based hybrid electrocatalysts for oxygen evolution, Angew. Chem. 58 (2019) 17458–17464.
[48] K. Zhu, X. Zhu, W. Yang, Application of in situ techniques for the characterization of NiFe-based oxygen evolution reaction (OER) electrocatalysts, Angew. Chem. 58 (2019) 1252–1265.
[49] P. Gao, Y. Zeng, P. Tang, Z. Wang, J. Yang, A. Hu, J. Liu, Understanding the synergistic effects and structural evolution of $Co(OH)_2$ and Co_3O_4 toward boosting electrochemical charge storage, Adv. Funct. Mater. 32 (2021) 2108644.
[50] M. Yu, E. Budiyanto, H. Tüysüz, Principles of Water Electrolysis and Recent Progress in Cobalt-, Nickel-, and Iron-Based Oxides for the Oxygen Evolution Reaction, Angew. Chem. Int. Ed. 61 (1) (2022) e202103824.
[51] D.L.A. de Faria, S. Venâncio Silva, M.T. de Oliveira, Raman microspectroscopy of some iron oxides and oxyhydroxides, J. Raman Spectrosc. 28 (11) (1997) 873–878.
[52] R.B. Penland, S. Mizushima, C. Curran, J.V. Quagliano, Infrared absorption spectra of inorganic coördination complexes. X. studies of some metal-urea complexes1a, b, J. Am. Chem. Soc. 79 (7) (1957) 1575–1578.
[53] H.B. Tao, Y. Xu, X. Huang, J. Chen, L. Pei, J. Zhang, J.G. Chen, B. Liu, A general method to probe oxygen evolution intermediates at operating conditions, Joule 3 (6) (2019) 1498–1509.
[54] R. Subbaraman, D. Tripkovic, K.-C. Chang, D. Strmcnik, A.P. Paulikas, P. Hirunsit, M. Chan, J. Greeley, V. Stamenkovic, N.M. Markovic, Trends in activity

for the water electrolyser reactions on 3d M(Ni Co, Fe, Mn) hydr(oxy)oxide catalysts, Nat. Mater. 11 (6) (2012) 550–557.
[55] A. Schranck, R. Marks, E. Yates, K. Doudrick, Effect of urine compounds on the electrochemical oxidation of urea using a nickel cobaltite catalyst: an electroanalytical and spectroscopic investigation, Environmental, Sci. Technol. 52 (15) (2018) 8638–8648.
[56] D.A. Daramola, D. Singh, G.G. Botte, Dissociation rates of urea in the presence of NiOOH catalyst: a DFT analysis, J. Phys. Chem. A 114 (43) (2010) 11513–11521.
[57] N.D. Dimas Suárez, K.M. Merz, Ureases: quantum chemical calculations on cluster models, J. Am. Chem. Soc. 125 (2003) 15324–15337.